iJDASE International Journal of Data Analytics and Smart Education

iJDASE | ISSN: 2736-979X | Vol. 1 No. 2 (2026)
https://doi.org/10.64817/wwmqn629

PAPER

# Assessing The Use of Artificial Neural Network for Feature Detection in Sentinel 2 and Landsat 8

**E. O. Makinde** ✉ [1],
**Abdul Hikmat T.** [1],
**Oyewole Ayomide P.** [1]

[1] Department of Surveying and Geo-Informatics, University of Lagos, Nigeria

eomakinde@unilag.edu.ng
abdulhikmat39@gmail.com
oyewoleayomide02@gmail.com

## ABSTRACT

Improved satellite imagery from recent remote sensing advances allows for more detailed classifications, although results differ based on the chosen algorithm and software. This study explores how well Artificial Neural Networks (ANNs) can identify features in Sentinel-2 and Landsat 8 satellite images, specifically focusing on land use and land cover (LULC) mapping and comparing ANN performance across the two datasets. The research methodology involves using identical training and validation datasets to ensure a fair comparison. The classified images are evaluated for accuracy using a confusion matrix, while change detection analysis is performed to assess land cover variations over time. The findings indicate that ANN delivers reliable results for both Sentinel-2 and Landsat 8 imagery, with higher accuracy observed in Sentinel-2 data. The change detection analysis reveals land cover dynamics, offering valuable insights into spatial and temporal patterns. This study advances remote sensing research by demonstrating the effectiveness of ANN in feature detection and its applicability to LULC mapping. The findings carry important implications for urban development, environmental conservation, and the monitoring of natural resources.

## KEYWORDS

Remote Sensing, Land Use, Land Cover Map, Change Detection, Artificial Neural Network.

E. O. Makinde, Abdul Hikmat T., Oyewole Ayomide P. (2026). Assessing The Use of Artificial Neural Network for Feature Detection in Sentinel 2 and Landsat 8. *International Journal of Data Analytics and Smart Education (iJDASE),* 1(2) pp. 1-40 https://doi.org/10.64817/wwmqn629

# 1 INTRODUCTION

The use of satellite imagery has greatly transformed our understanding of global challenges, especially in areas like disaster response and climate change monitoring. This change is driven by advancements in computer vision, deep learning, and the increasing availability of cost-effective, high-performance GPUs. The rising focus on detecting objects in aerial images reflects these technological breakthroughs, paralleling significant progress in fields such as image processing, pattern recognition, and machine learning. The crux of this advancement lies in the identification and description of image features [1].

The practical application of these technologies in low-resource settings remains limited by several challenges, including the lack of access to high-quality labeled data, inadequate internet infrastructure, limited computational power, and insufficient technical expertise. For instance, [27] emphasize that in regions with fragmented or heterogeneous landscapes, high classification errors are common due to spectral confusion. Similarly, [28] highlight that large-scale cloud-based platforms like Google Earth Engine, while transformative, are often underutilized in developing countries due to connectivity and training barriers. These issues are further exacerbated in socio-economically disadvantaged areas where satellite-based models may not generalize well due to land-use dynamics not captured in training datasets. The crux of this advancement still lies in the identification and description of image features, but its global utility depends on addressing these implementation challenges.

Societal progress hinges on socioeconomic development. Consequently, comprehensive socio-economic evaluations, encompassing both spatial and non-spatial datasets, are conducted. Central to this approach are Land Use/Land Cover (LULC) maps, which play a pivotal role in program planning, management, and monitoring at local, regional, and national scales [2]. While the terms "land use" and "land cover" are often used interchangeably, they bear distinct definitions. "Land cover" encompasses the physical elements on Earth's surface, while "land use" signifies the economic purpose. However, a nexus exists between these two domains. Typically, classes of land parcels serve as the foundation for constructing land use and land cover maps [3]. When "Land Use" and "Land Cover" are used concomitantly, they denote the classification of human activities and natural elements using established scientific and statistical methods [3].

Despite their utility, LULC maps face several limitations. Mapping accuracy is often compromised in heterogeneous landscapes such as forests transitioning to agricultural land, wetlands, or peri-urban zones due to spectral similarity and the prevalence of mixed pixels [29]. In rapidly urbanizing areas, the fast pace of land transformation demands higher temporal resolution, which many satellite systems cannot meet [30]. In addition, cloud cover, seasonal variability, and a lack of consistent ground-truth data particularly in developing countries can significantly degrade classification reliability [31]. These challenges not only impact the accuracy

of land cover classifications but also limit the effectiveness of change detection and long-term environmental monitoring.

The trajectory of satellite data, characterized by medium to high resolutions, has been propelled by advancements in remote sensing technology. This has spawned a new generation of image classification algorithms, with accessibility across diverse domains driving this evolution [4]. Notably, different classifiers exhibit distinct operational procedures, leading to varied outcomes based on the classifier and software capabilities. However, the performance of these algorithms varies across landscapes. For instance, SVM is known to perform exceptionally well in high-dimensional, sparse feature spaces like desert or mountainous terrains with fewer training samples [32]. Random Forest, by contrast, has shown strong accuracy in highly heterogeneous or fragmented urban and agro-pastoral landscapes due to its ensemble decision-tree mechanism [33]. KMeans and ISODATA, while useful in unsupervised contexts, tend to perform poorly in spectrally complex environments like tropical forests or rapidly urbanizing zones where class boundaries are ambiguous [34]. Therefore, algorithm selection should consider both the ecological context and the availability of training data to optimize classification accuracy and efficiency.

Supervised and unsupervised algorithms find utility in this context. Unsupervised methods, as illustrated by KMeans [5] and ISODATA [6], cluster data based on reflection properties without site-specific input data [7]. Conversely, supervised algorithms, exemplified by minimum distance[8], and maximum likelihood [9], rely on user-assigned spectral signatures for class distinction[10]. The selection of training data and final outcomes involves human influence and bias. Notably, supervised algorithms, including minimum distance [11], maximum likelihood [12], artificial neural network, [13], random forest [14], and support vector machine [15], exhibit superior accuracy due to their robust class distinction capabilities [16],[17]. In recent years, advanced machine learning (ML) methods have gained favor, especially in predicting natural hazards like floods, snow avalanches, and landslides [18], owing to their enhanced accuracy and flexibility [19],[20]. The adoption of these models is witnessing an upsurge in the production of accurate LULC maps. ML demonstrates competence in managing classification scenarios, and the relevance of Neural Networks escalates when addressing a substantial number of output classes and voluminous datasets [1]

Artificial Neural Networks (ANNs) stand as a distinctive category of machine learning algorithms designed to emulate human brain function. These networks, similar to neurons in the nervous system, possess the ability to learn from past data and offer predictions or classifications. A significant advantage of ANNs is their capacity to generate output results from sample data, obviating the need for the entire dataset. ANNs enhance current data analysis methodologies by revealing intricate connections between inputs and outputs, unlocking novel patterns. Their applications span diverse domains, encompassing image recognition, speech recognition, machine translation, and medical diagnosis [1]. Despite these

advantages, applying ANNs to satellite imagery involves several challenges. One major constraint is the need for large volumes of high-quality labeled training data to effectively learn feature relationships something often unavailable in data-scarce regions or for rare land cover class. Additionally, due to their complexity and high number of parameters, ANNs are prone to overfitting, especially when trained on small or imbalanced datasets [35]. To mitigate this, techniques like dropout, early stopping, or regularization must be carefully implemented. Moreover, the training of deep ANNs, particularly convolutional neural networks (CNNs), demands substantial computational power often requiring GPUs or cloud-based platforms, which may be inaccessible in resource-limited settings [36]. As such, while ANNs are powerful tools for satellite image classification, their effective deployment depends on data availability, model tuning, and computational infrastructure.

The surge in accessibility to high-resolution satellite imagery, typified by Landsat and Sentinel-2, is redefining local and national applications like urban planning, agriculture, and natural resource management. Notably, the US Geological Survey's open data policy (Woodcock, 2008) and the European Space Agency's Copernicus program are pivotal in democratizing satellite data access. Landsat's role in the scientific community has witnessed exponential growth following the policy's enactment, particularly benefiting areas with data scarcity and economic challenges. Landsat 8's launch in 2013 has bolstered spectral capabilities, enabling its integration into global-scale LULC and natural resource mapping [21],[22]. Sentinel-2, developed under the Copernicus program and launched in 2015, offers 13 spectral bands at varying spatial resolutions (10 m, 20 m, 60 m), enabling fine-grained environmental monitoring. While both satellites are valuable, they exhibit performance differences in specific contexts. Sentinel-2, with its higher spatial and temporal resolution (5-day revisit with dual satellites), excels in detecting urban sprawl, delineating field boundaries, and mapping small agricultural plots [37],[38]. Landsat 8, in contrast, offers superior radiometric calibration and a longer historical data record, making it ideal for long-term environmental change detection and global forest monitoring [39]. In agricultural settings, Sentinel-2 outperforms Landsat 8 in identifying crop types and phenological stages, while Landsat's stable calibration and thermal bands offer advantages for evapotranspiration and drought monitoring [40]. These strengths make the two sensors complementary rather than competitive, depending on the temporal, spatial, and thematic needs of a study.

Moreover, the European Space Agency's initiative, manifested in satellite sensors like Sentinel-2A (S-2), underscores the commitment to free satellite image dissemination to scientific, governmental, and private sectors [23]. Sentinel-2A, launched in 2015, delivers multi-spectral imagery across varied spatial resolutions, spanning visible and near-infrared bands to atmospheric correction bands [23].
The convergence of satellites with high spatial and spectral resolutions has invigorated remote sensing grounded in image categorization. This intersection has propelled remotely sensed data, informed by machine learning classification algorithms, as an efficacious method for analyzing land cover and extracting its inherent properties. Against this backdrop, the study aims to meticulously compare

classification and accuracy results from Sentinel-2 and Landsat 8 intermediate-resolution satellites. This will be accomplished by employing consistent training sites, samples, and timeframe parameters, elucidating the landscape of modern satellite-based image analysis [1].

## 2 STUDY AREA

Abuja is located in the North-Central part of Nigeria, and lies between within latitudes 9°24'32.91"N and 8°29'15.60"N and longitude 6°47'16.23"E and 7°38'52.55"E. It is the capital and eighth-most populous city of Nigeria. Abuja, the capital of Nigeria, is centrally located within the Federal Capital Territory and was developed as a planned city in the 1980s based on a master plan by Japanese architect Kenzo Tange. It officially replaced Lagos as the nation's capital on December 12, 1991.

Aso Rock, a 400-meter (1,300 ft) monolith shaped by water erosion, is a defining feature of Abuja's landscape, with key government institutions such as the Presidential Complex, National Assembly, and Supreme Court positioned to its south. North of the city, along the Kaduna expressway, stands Zuma Rock, a striking 792-meter (2,598 ft) monolith. According to the 2006 census, Abuja had a population of 776,298, ranking it as the eighth most populous city in Nigeria at the time.

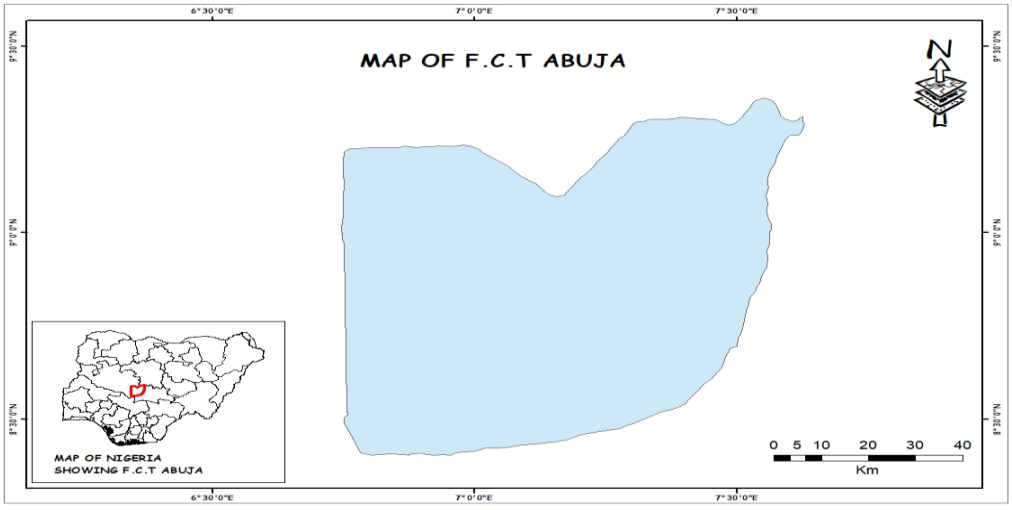


**Fig. 1: Map of Abuja**

# 3 NETWORK ANALYSIS

The primary categories of the software to be used for this project are; Microsoft Word 2013, Microsoft PowerPoint, SNAP, ArcGIS 10.4, ArcGIS Pro 3.0, and Google Earth.

## 3.1 Route Analysis (Network Analysis for Optimal Path)

The data acquired are Landsat 8 and Sentinel 2

### 3.1.1 Landsat 8

Satellite data from Landsat 8 was used to study changes over time. Images were taken every two years from 2016 to 2022 and downloaded from the USGS Earth Explorer website. The satellite is equipped with the Operational Land Imager (OLI) and the Thermal Infrared Sensor (TIRS). The TIRS sensor includes two spectral bands (10 and 11) for thermal imaging, aligned with OLI's nine spectral bands (bands 1–9) covering the visible, near-infrared (NIR), and shortwave infrared (SWIR) regions. The study area was fully captured within a single tile, Path 189 and Row 54.

The Landsat 8 imagery used in this study was obtained from the USGS Earth Explorer in Level-1 and Level-2 Surface Reflectance products, which are already atmospherically corrected using the Landsat Surface Reflectance Code (LaSRC). To ensure data quality, scenes were selected with cloud cover <10%. Additionally, the Quality Assessment (QA) bands provided with the product were used to mask residual clouds, cloud shadows, and snow pixels, ensuring that only valid surface reflectance values were used for classification.

A two-year interval was selected to balance temporal resolution with processing complexity, ensuring sufficient sensitivity to land cover changes without data overload. This interval also coincides with seasonal and climatic cycles in the region, allowing patterns of gradual transformation—particularly in vegetation and urban expansion—to emerge clearly. While shorter intervals (e.g., annually) were considered, they were excluded due to increased noise from seasonal variability and cloud interference, as well as limitations in cloud-free image availability.

To maintain data quality and minimize atmospheric distortion, a cloud cover threshold of <10% was used during image selection. This limit is widely adopted in remote sensing to reduce classification errors caused by cloud obstruction and shadows (Zhu & Woodcock, 2012). Even minor cloud presence can mask land surface features and lead to misclassification, especially in spectral bands used for vegetation and water detection. In highly dynamic land surfaces like those in Abuja, ensuring minimal cloud contamination was critical to reliable change detection.

The percentage cloud cover is a critical parameter of remote sensing since the shadow and the clouds themselves can cover up the features of the ground making

the process of classifying the ground cover type not easy. This paper used a threshold of less than 10 percent as it limits cloud pollution and gives a clear view of the earthly features. The lower this limit kept the cloud cover, the better the classification results are reliable and minimal errors made in successive analyses like change detection. The number of percent of the satellite image that is covered by the clouds is the Scene Cloud Cover and the percentage of the terrestrial area covered by clouds is the Land Cloud Cover. They were both limited to less than 10 percent to ensure the integrity of data in terms of classification.

**Table 1: List of the Selected Landsat-8 Images for the Study Area**

| Landsat Product Identifier | Sensing Date | Scene Cloud Cover | Land Cloud Cover |
|---|---|---|---|
| LC08_L1TP_189054_20180116_20200902_02_T1 | 16 December 2018 | 0.97 | 0.97 |
| LC08_L2SP_188054_20201114_20210315_02_T1 | 14 November 2020 | 0.60 | 0.52 |
| LC08_L1TP_189054_20221229_20230104_02_T | 29 December 2022 | 0.02 | 0.02 |

### 3.1.2 Sentinel 2

Sentinel 2 data for the same period of years as the Landsat 8 data (i.e2018, 2020, 2022) was downloaded freely from Copernicus Scientific Data Hub website (https://www.copernicus.eu/en/access-data/conventional-data-access-hubs). Four tiles of Sentinel-2 cover the whole study area and the cloud cover range was set < 10. Table 2 presents the details of data acquired.

A user account was created on the Copernicus data hub website before gaining access to the Sentinel data.

Sentinel-2: The Sentinel-2 data was downloaded as Level-2A surface reflectance products from the Copernicus Open Access Hub, which are preprocessed with atmospheric correction (Sen2Cor). This preprocessing corrects for aerosol, water vapor, and ozone effects, delivering surface reflectance values ready for analysis. As with Landsat 8, scenes were filtered to cloud cover <10%, and the Scene Classification Layer (SCL) generated by Sen2Cor was used to mask clouds, shadows, and cirrus contamination.

General Preprocessing Steps:

- All imagery was subset to the study area and re-projected into a common coordinate reference system (WGS 84 / UTM Zone 32N).

- Radiometric and atmospheric corrections were applied via the Level-2A and Level-2SP products.
- Cloud and shadow pixels were masked out using the QA bands (Landsat) and SCL masks (Sentinel-2).
- The resulting clean, surface reflectance datasets were then used to generate training signatures for supervised classification with the Artificial Neural Network (ANN).

**Table 2: List of the Selected Sentinel Images for the Study Area**

| Year | Granule ID | Sensing Date | Cloud cover percentage | Cloud shadow percentage |
|---|---|---|---|---|
| 2018 | S2A_MSIL2A_20181229T095411_N0211_R079_T32PLQ_20181229T121118 | 29 December 2018 | 7.264047 | 0.0 |
| | S2A_MSIL2A_20181229T095411_N0211_R079_T32PLR_20181229T121118 | 29 December 2018 | 7.264047 | 0.0 |
| | S2B_MSIL2A_20181214T095409_N0211_R079_T32PKQ_20181214T140003 | 14 December 2018 | 0.039993 | 0.0 |
| | S2B_MSIL2A_20181214T095409_N0211_R079_T32PKR_20181214T140003 | 14 December 2018 | 0.223519 | 1.7E-5 |
| 2020 | S2A_MSIL2A_20201113T095351_N0213_R079_T32PLR_20200113T115210 | 13 November 2020 | 0.001425 | 0.0 |
| | S2A_MSIL2A_20201218T095421_N0214_R079_T32PKR_20201218T120639 | 18 December 2020 | 0.175829 | 2.3E-5 |
| | S2A_MSIL2A_20201113T095351_N0213_R079_T32PKQ_20200113T115210 | 13 November 2020 | 0.427009 | 0.0 |
| | S2A_MSIL2A_20201218T095421_N0214_R079_T32PLQ_20201218T120639 | 18 December 2020 | 3.693801 | 1.8E-3 |
| 2022 | S2A_MSIL2A_20221228T095421_N0509_R079_T32PLR_20221228T144254 | 28 December 2022 | 3.09E-4 | 0.0 |
| | S2A_MSIL2A_20221208T095411_N0509_R079_T32PKQ_20221208T144756 | 08 December 2022 | 0.01121 | 0.0 |
| | S2A_MSIL2A_20221208T095411_N0509_R079_T32PLQ_20221208T144756 | 08 December 2022 | 2.253624 | 6.1E-5 |
| | S2A_MSIL2A_20221118T095311_N0400_R079_T32PKR_20221118T145555 | 11 November 2022 | 7.264047 | 0.0 |

The sentinel-2 imagery gives multispectral data with a spatial resolution of 10 m, 20 m and 60 m based on the spectral band. To carry out this research, 10 m and 20 m bands were mainly used to aid more detailed classification of land cover. Nevertheless, the use of four tiles added more processing procedures such as mosaicking and radiometric harmonization to provide the same coverage of the study area. A free user account was created on the Copernicus Data Hub to access and download the Sentinel-2 imagery, as this is a standard requirement for obtaining datasets from the platform. This practical step ensures that researchers can easily replicate the data acquisition process for their own studies. Cloud shadow percentage is the percentage of the image that is covered by cloud shadows and

similar to cloud cover, it can cause reduced visibility of features on the ground. Priority was given to low cloud shadow values to reduce errors of misclassification during the analysis of land cover.

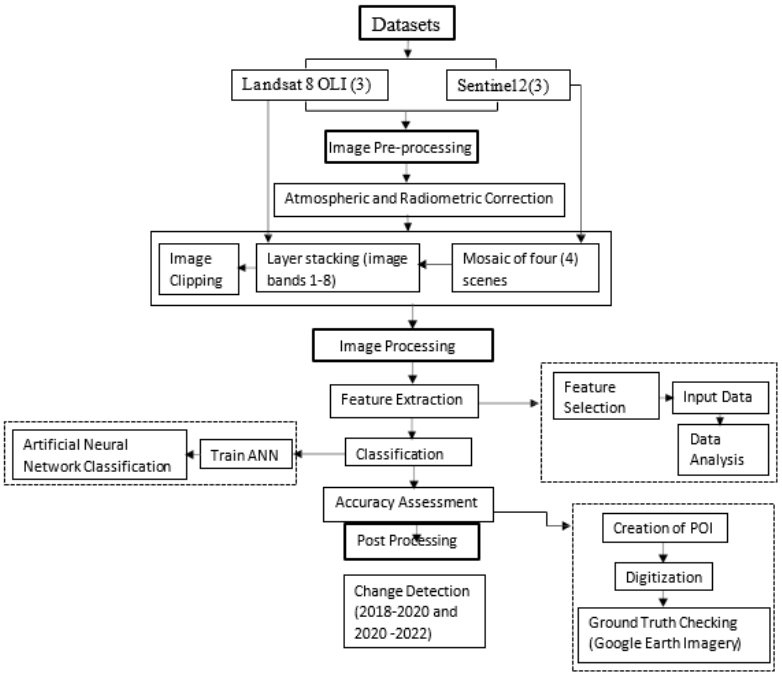


**Fig. 2: Flowchart of the study**

Although both the Landsat 8 and Sentinel-2 datasets used were filtered to ensure that the proportion between cloud cover and cloud shadow is not above 10 per cent, the way they were processed to address atmospheric conditions is slightly different. Sentinel-2, which has a better spatial resolution and more spectral bands, is more successful in separating clouds and shadows and land features. By comparison, Landsat 8 has a lower resolution, and atmospheric artifacts can sometimes be left by the resolution, thereby affecting classification quality. This is a consideration which does imply the need to have uniform filtering thresholds in each dataset in order to make a comparison.

Cloud cover is a direct effect on the quality of satellite images as it hides the features on the ground and creates noise in the final classification outputs. Huge percentages of cloud can result in incorrect classification of land cover types, and the shadows of clouds can look like dark surfaces, such as water or bare soil, and hence decrease the accuracy of classification. Limiting the accepted images to less than 10 percent cloud cover, this work guaranteed the better visibility of the land characteristics, reduced atmospheric interference, and enhanced the precision of the land cover mapping and further analysis of change detection.

The choice of Landsat 8 and Sentinel-2 was based on the fact that they have complementary capabilities in terms of medium and high-resolution observation of the Earth. Landsat 8, released in 2013 offers 30 m resolution in the majority of bands (including 15 m panchromatic band) and has a 16-day revisit cycle, and hence suitable in long-term change detection. When both Sentinel-2A and 2B are operational, sentinel-2 provides finer spatial resolutions of 10 m, 20 m, and 60 m depending on the band, and can give a 5-day revisit cycle. With the combination of these datasets, it is possible to effectively compare the classification performance within different resolutions and between different time periods, which fits the purposes of the present study which is feature identification and LULC mapping.

### 3.2 Image Classification

Image classification entails assigning land cover categories to individual pixels, involving the extraction of distinct information classes from a multiband raster image. This procedure culminates in the creation of Land Use Land Cover (LULC) maps through the utilization of the raster generated from the image classification process. The manner in which the analyst and the computer collaborate during classification determines the outcome. This study's image classification process was undertaken by adhering to the following protocol:

- Create Training Set
  The different training datasets representing surface cover types were identified. Five classes were selected such as Built-up, Bare land, Vegetation, Wetland Rangeland, and average of 7 samples were created for each class

- Develop a Signature File
  The signature file was created by inputting the raster image and the training classes in the spatial analyst tool that generate signature file
  A signature file is simply a set of spectral profiles of all the land cover classes, which are based on training samples. The different surfaces types (e.g., vegetation, built-up, water) absorb and reflect light in dissimilar ways within the various spectral bands of the satellite. These reflectance values stored in a signature file assist in identifying and assigning each pixel in the image to the most probable land cover classification by the classifier (ANN in this instance). This is an important step since it converts the raw satellite data into a spectrophotometric library, which is used to lead the classification procedure. In order to verify that the training samples were spectrally different, a spectral separability test might be conducted with the help of spectral separability evaluation metrics, like the Jeffries-Matusita (JM) distance or the Transformed Divergence (TD). These measures evaluate the quality of separation of classes in spectral space and values of 2.0 (JM) or >1900 (TD) are good evidence of the quality of separation. Although ANN can work on non-linear class boundaries, spectral separability analysis would

further give a validation step to ensure that the training samples sufficiently capture different land cover classes.

- Classify Image
  The image was classified by training Artificial Neural Network algorithm
  The five land cover types; Built-up, Bare Land, Vegetation, Wetland and Rangeland were chosen because they are the most common surface types in the Abuja region. The categories are specifically applicable to the tracking of urban growth, vegetation dynamics, and land resource use, which, in turn, fully correlates with the aim of the current study, which is to assess the changes in LULC and be used in the fields of environmental monitoring and urban planning.
  The signature file was produced in ArcGIS through the extension of Spatial Analyst. Each land cover class training sample was digitized in the form of polygons and spectral signatures were created with the help of the Create Signature File tool. Spectral separability and minimum sample size (≥7 polygons per class) parameters were verified to verify that the signature is of high quality and can be utilized in supervised classification.
  ANN was selected due to its capability of describing complex and non-linear associations between spectral data, and it is most suitable when applied to non-homogenous landscapes like Abuja. ANN offers strong classification with minimal assumptions about the data distribution compared to Support Vector Machines (SVM), which need both the choice of the kernel, and parameter tuning, and Random Forest (RF), which can easily overfit on small samples. Past researches also have shown that ANN can perform well in LULC mapping particularly where two or more types of land cover exist in the same scene [41].

### 3.2.2 Algorithm of Artificial Neural Networks

The Artificial Neural Network (ANN) algorithm, modeled after the complex neural structures of the human brain, functions as a powerful nonlinear modeling tool capable of solving problems without relying on predefined assumptions. This characteristic equips it to discern intricate relationships within various types of input data. This methodology finds widespread utility across diverse domains, including tasks like landslide susceptibility mapping (LSM), landslide detection, and classification. Artificial neural Network (ANN) was used on a multilayer perceptron (MLP) architecture with the following parameters: Input Layer: Spectral bands used (e.g. 6-10 depending on data) are equal to number of neurons. Hidden Layer(s): A single hidden layer containing X neurons (e.g., 1015), that is selected via trial and error to achieve a compromise between performance and overfitting. Activation Function: sigmoid hidden layer neurons and softmax output classification. Learning Rate: 0.01 Training Algorithm: Backpropagation using adaption learning rate. Epochs (iterations): 1,000 Output Layer: There are six neurons that represent the six LULC classes (vegetation, rangeland, bare land, built-up, bare hill surface, waterbody).

The fundamental configuration of this approach comprises three distinct layers. The initial layer is dedicated to data input. The second layer, often referred to as the hidden layer, applies essential computations to the data. These computations hinge on processing elements known as neurons. The number of neurons is determined by users through a trial-and-error process. The concluding layer defines the ultimate outputs.

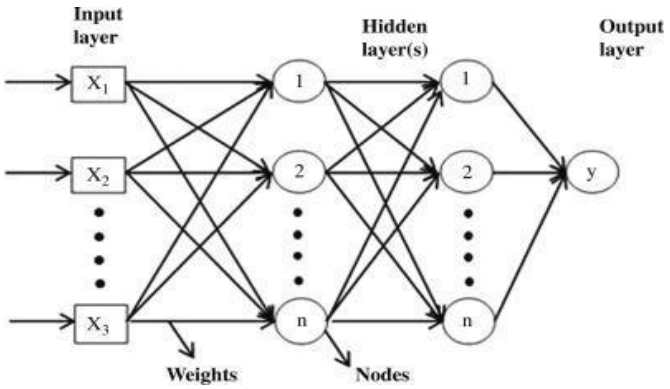


**Fig. 3: Architecture of ANN**

The training structure of this network unfolds as follows: training samples are fed into the network through the input layer, subsequently advancing to the intermediary layer by being multiplied with the connecting weights associated with neurons. Within the intermediary layer, neurons perform necessary computations before transmitting the resultant values to the output layer. Weights and biases are ascertained via a non-linear optimization process known as training. This training process seeks to minimize a learning function, aimed at establishing proximity between the observed data and the output produced by the ANN.

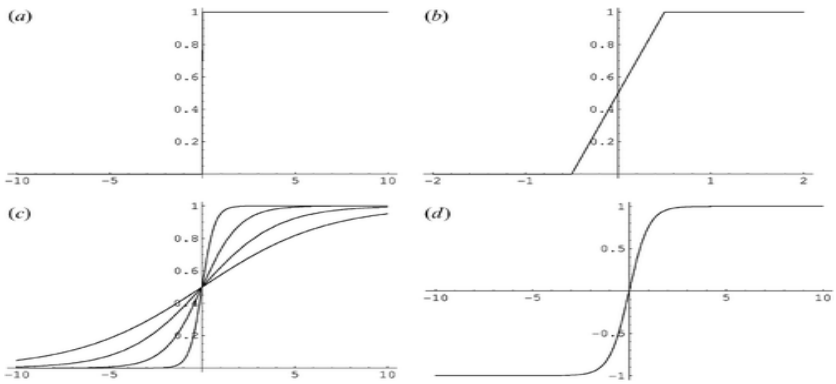


**Fig. 4: Activation Functions: (a) Threshold, (b) Piecewise-Linear, (c) Logistic (Sigmoid) and (d) Hyperbolic.**

ANN also has flaws to image classification despite its benefits. The quality and quantity of training data determine the effectiveness of the algorithm greatly; both

underrepresented and insufficient samples may result in the decrease of its accuracy. ANN is also vulnerable to atmospheric and residual cloud contamination, which can cause noise to spectral signatures. These difficulties underscore the fact that preprocessing should be carefully done and sufficient training samples should be chosen so as to have reliable classification results [42]. The size of the hidden layer was set by trial-and-error and a small number of neurons was initially taken (5 neurons) and then added until the classification level was no longer improving but fluctuations of overfitting were observed. All the structures were tested with validation data and the best structure was chosen when adding more neurons did not help to increase the accuracy of classification. The backpropagation method was used with a learning rate of 0.01 and a maximum number of iterations of 1,000, as these are common values when performing LULC classification tasks

# 4 RESULTS AND DISCUSSION

## 4.1 Image Classification

### 4.1.1 Image Classification for the Landsat 8 Imageries

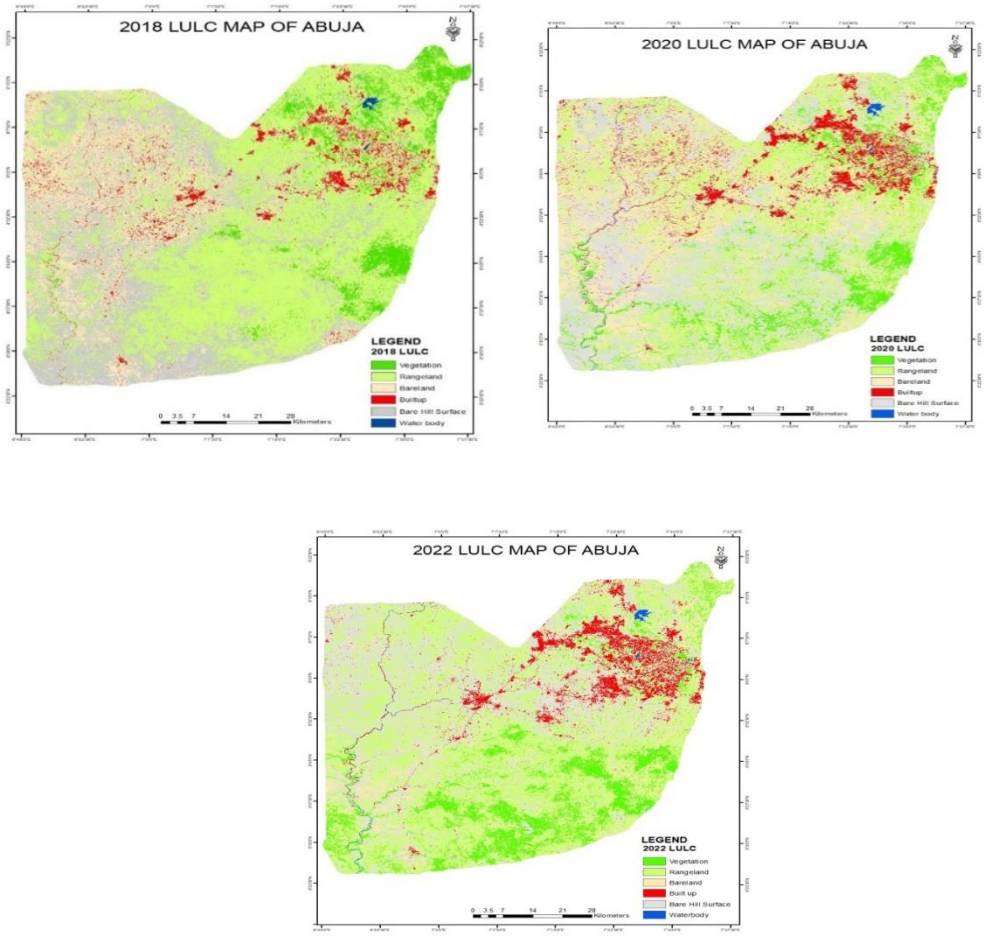


**Fig. 5: 2018, 2020, and 2022, Classified Landsat 8 Imagery of Abuja respectively**

The Sentinel-2 2018, 2020, and 2022 classification depict evident spatial and temporal differences between the land use/land cover (LULC) of Abuja. In the three epochs, the landscape of vegetation and built-up areas is steadily prevailing, and built-up areas are steadily on the rise since 2018 to 2022. The rapid urbanization of Abuja is reflected by this growth especially along the central areas and the peri-urban peripheries. On the other hand, rangeland and bare hill surfaces show a slow progressive degradation implying conversion of open or undeveloped land into residential and infrastructural amenities.

### 4.1.2 Image Classification for the Sentinel 2 Imageries

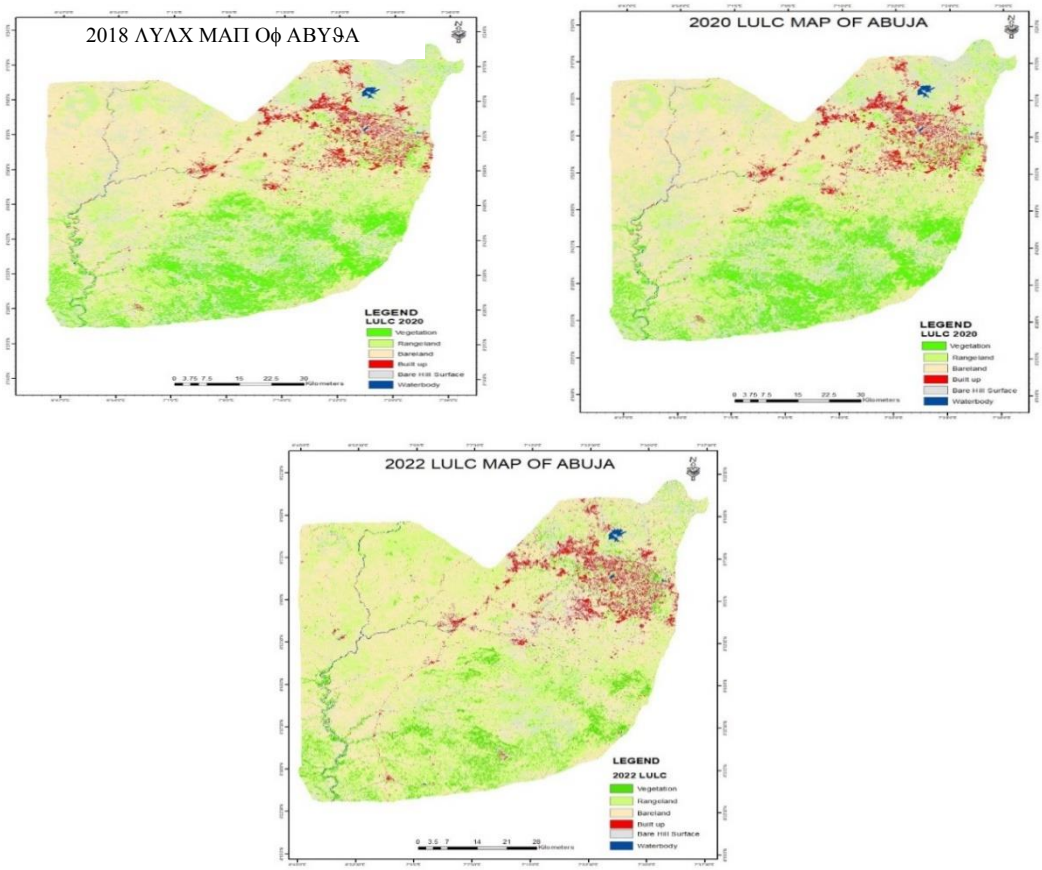


**Fig. 6: 2018, 2020, and 2022, Classified Sentinel 2 Imagery of Abuja respectively**

Classification results also reveal the seasonal and inter-annual variations in vegetation cover which possibly are due to the natural phenological variations as well as human disturbances like agriculture and construction. The wetlands and water bodies were also found to be fairly constant in area but a few minimal changes were experienced along the river courses which could be attributed to the seasonal changes in water level. The results of these observations are supported by the accuracy assessment results, as the overall accuracies of Sentinel-2 data were 78.33, 83.33 and 86.7 per cent in 2018, 2020 and 2022 respectively, with Kappa coefficients

between 0.76 and 0.84, which is substantial to near-perfect agreement. The same trend of progressive accuracy improvement with time can be attributed to the quality of the training sample and the capability of the ANN classifier to learn any sophisticated spectral pattern in subsequent dataset.

## 4.2 Accuracy Assessment for Sentinel 2 Imageries

### 4.2.1.1 2018 Sentinel 2 Accuracy Assessment

**Table 3: 2018 Sentinel 2 Accuracy Assessment Table**

| | Vegetation | Range Land | Bare land | Built up | Bare Hill Surface | Waterbody | Total User | User Accuracy | Kappa Co-efficient |
|---|---|---|---|---|---|---|---|---|---|
| Vegetation | 9 | 1 | 0 | 0 | 0 | 0 | 10 | 0.9 | 0 |
| Range Land | 0 | 9 | 0 | 0 | 1 | 0 | 10 | 0.9 | 0 |
| Bare land | 0 | 3 | 7 | 0 | 0 | 0 | 10 | 0.7 | 0 |
| Built Up | 0 | 1 | 1 | 8 | 0 | 0 | 10 | 0.8 | 0 |
| BareHill Surface | 0 | 3 | 2 | 0 | 6 | 0 | 10 | 0.5 | 0 |
| Waterbody | 0 | 0 | 1 | 0 | 0 | 9 | 10 | 0.9 | 0 |
| Total Producer | 9 | 17 | 11 | 8 | 7 | 9 | 60 | 0 | 0 |
| Producer Accuracy | 1 | 0.529412 | 0.636364 | 1 | 0.833333 | 1 | 0 | 0.79 | 0 |
| Kappa Co-efficient | 0 | 0 | 0 | 0 | 0 | 0 | 0 | 0 | 0.76 |

$$\text{Overall Accuracy} = \frac{\text{Total Number of Correctly Classified Pixels in each Category}}{\text{Total Numer of Reference Pixels}} \times 100 \quad (1)$$

$$\text{Overall Accuracy} = \frac{48}{60} \times 100 = 78.33\%$$

$$\text{Kappa coefficient} = \frac{(\text{TS} \times \text{TCS}) - \sum(\text{Column Total} \times \text{Row Total})}{\text{TS2} - \sum(\text{Column Total} - \text{Row Total})} \times 100 \quad (2)$$

$$\text{Kappa coefficient} = 76\%$$

The kappa coefficient is substantial (i.e. very good)

#### 4.2.1.2 2020 Sentinel 2 Accuracy Assessment

**Table 4: Accuracy Assessment Table 2020**

| | Vegetation | Range Land | Bare land | Built up | Bare Hill Surface | Waterbody | Total User | User Accuracy | Kappa Co-efficient |
|---|---|---|---|---|---|---|---|---|---|
| Vegetation | 9 | 1 | 0 | 0 | 0 | 0 | 10 | 0.9 | 0 |
| Range Land | 2 | 8 | 0 | 0 | 0 | 0 | 10 | 0.8 | 0 |
| Bare land | 0 | 2 | 8 | 0 | 0 | 0 | 10 | 0.8 | 0 |
| Built Up | 0 | 0 | 0 | 9 | 0 | 1 | 10 | 0.9 | 0 |
| Bare Hill Surface | 1 | 1 | 2 | 0 | 6 | 0 | 10 | 0.6 | 0 |
| Waterbody | 0 | 0 | 0 | 0 | 0 | 10 | 10 | 1 | 0 |
| Total Producer | 12 | 12 | 10 | 9 | 6 | 11 | 60 | 0 | 0 |
| Producer Accuracy | 0.75 | 0.666667 | 0.8 | 1 | 1 | 0.909091 | 0 | 0.833333 | 0 |
| Kappa Co-efficient | 0 | 0 | 0 | 0 | 0 | 0 | 0 | 0 | 0.8 |

$$\text{Overall Accuracy} = \frac{\text{Total Number of Correctly Classified Pixels in each Category}}{\text{Total Numer of Reference } \mathbf{Pixels}} \text{ x } 100 \quad (3)$$

$$\text{Overall Accuracy} = \frac{50}{60} \text{ x } 100 = 83.3\%$$

$$\text{Kappa coefficient} = \frac{(\text{TS x TCS}) - \sum (\text{Column Total x Row Total})}{\text{TS2} - \sum (\text{Column Total} - \text{Row Total})} \text{ x } 100 \quad (4)$$

$$\text{Kappa coefficient} = 80\%$$

The kappa coefficient is substantial (i.e. very good)

#### 4.2.1.3 2022 Accuracy Assessment

**Table 5: 2022 Sentinel Accuracy Assessment Table**

| | Vegetation | Range Land | Bare land | Built up | Bare Hill Surface | Waterbody | Total User | User Accuracy | Kappa Co-efficient |
|---|---|---|---|---|---|---|---|---|---|
| Vegetation | 10 | 0 | 0 | 0 | 0 | 0 | 10 | 1 | 0 |
| Range Land | 0 | 10 | 0 | 0 | 0 | 0 | 10 | 1 | 0 |
| Bare land | 0 | 1 | 9 | 0 | 0 | 0 | 10 | 0.9 | 0 |
| Built Up | 0 | 0 | 0 | 10 | 0 | 0 | 10 | 1 | 0 |
| Bare Hill Surface | 0 | 2 | 2 | 1 | 5 | 0 | 10 | 0.5 | 0 |
| Waterbody | 0 | 0 | 0 | 2 | 0 | 8 | 10 | 0.8 | 0 |
| Total Producer | 10 | 13 | 11 | 13 | 5 | 8 | 60 | 0 | 0 |
| Producer Accuracy | 1 | 0.769231 | 0.818182 | 0.769231 | 1 | 1 | 0 | 0.866667 | 0 |
| Kappa Co-efficient | 0 | 0 | 0 | 0 | 0 | 0 | 0 | 0 | 0.84 |

$$\text{Overall Accuracy} = \frac{\text{Total Number of Correctly Classified Pixels in each Category}}{\text{Total Numer of Reference } \mathbf{Pixels}} \text{ x } 100 \quad (5)$$

$$\text{Overall Accuracy} = \frac{52}{60} \text{ x } 100 = 86.7\%$$

$$\text{Kappa coefficient} = \frac{(\text{TS x TCS}) - \sum (\text{Column Total x Row Total})}{\text{TS2} - \sum (\text{Column Total} - \text{Row Total})} \text{ x } 100 \quad (6)$$

$$\text{Kappa coefficient} = 84\%$$

The kappa coefficient is almost perfect agreement i.e. Excellent

**Table 6:** 2018 Sentinel 2 User Accuracy Percentage

| Class Name | User Accuracy Percentage |
|---|---|
| Vegetation | 90% |
| Rangeland | 90% |
| Bare land | 70% |
| Built up | 80% |
| Bare Hill Surface | 50% |
| Water Body | 90% |

**Table 7:** 2018 Sentinel 2 Producer Accuracy Percentage

| Class Name | User Accuracy Percentage |
|---|---|
| Vegetation | 100% |
| Rangeland | 52.9% |
| Bare land | 63.63% |
| Built up | 100% |
| Bare Hill Surface | 83.33% |
| Water Body | 100% |

**Table 8:** 2020 Sentinel 2 User Accuracy Percentage

| Class Name | User Accuracy Percentage |
|---|---|
| Vegetation | 90% |
| Rangeland | 80% |
| Bare land | 80% |
| Built up | 90% |
| Bare Hill Surface | 60% |
| Water Body | 100% |

**Table 9:** 2020 Sentinel 2 Producer Accuracy Percentage

| Class Name | Producer Accuracy Percentage |
|---|---|
| Vegetation | 75% |
| Rangeland | 66.67% |
| Bare land | 80% |
| Built up | 100% |
| Bare Hill Surface | 100% |
| Water Body | 90.9% |

**Table 10:** 2022 Sentinel 2 User Accuracy Percentage

| Class Name | User Accuracy Percentage |
|---|---|
| Vegetation | 100% |
| Rangeland | 100% |
| Bare land | 90% |
| Built up | 100% |
| Bare Hill Surface | 50% |
| Water Body | 80% |

**Table 11:** 2022 Sentinel Producer Accuracy Percentage

| Class Name | Producer Accuracy Percentage |
|---|---|
| Vegetation | 100% |
| Rangeland | 76.9% |
| Bare land | 81.81% |
| Built up | 76.92% |
| Bare Hill Surface | 100% |
| Water Body | 100% |

The Kappa coefficient is specifically significant since it examines the degree of correlation among the classification outcomes and reference data more than what would happen exclusively by chance. Values falling in the range of 0.61 to 0.80 are usually treated as a high level of agreement whereas values above 0.80 are almost absolute agreement. Thus, the fact that 0.76 (2018) was picked up to 0.84 (2022) proves the fact that the classification not only became more accurate in general but more precise in differentiating classes of land covers over the time. One can also derive more by the Producer and User Accuracy values reported under each of the classes. Producer accuracy measures the proportion between the real-world features that are correctly assigned to a category (omission errors) and user accuracy measures the probability that a pixel that is assigned to a category actually represents the category on the ground (commission errors). As an illustration, the Built-Up class had a high user accuracy, and a lower producer accuracy in the 2018 classification meaning that in cases where the model classified an area as built-up, the model was often right, but not all built-up areas were detected, and therefore, the Built-Up class was under-represented. Vegetation class, on the other hand, showed little misclassification with a high producer and user accuracies. These findings indicate that the ANN classifier works well on average, but certain land cover classes, in particular, transitional or heterogeneous classes, (like Bare Hill Surface) are still harder to classify, presumably because they are spectrally similar to neighboring classes. In future analyses, these errors could be reduced by targeted refinement of training samples or by adding more spectral indices (e.g. NDVI as a vegetation discrimination index).

### 4.2.2 Accuracy Assessment for Landsat 8 Imageries

#### 4.2.2.1 2018 Landsat 8 Accuracy Assessment

**Table 12: 2018 Landsat 8 Accuracy Assessment Table**

| | Vegetation | Range Land | Bare land | Built up | Bare Hill Surface | Waterbody | Total User | User Accuracy | Kappa Co-efficient |
|---|---|---|---|---|---|---|---|---|---|
| Vegetation | 9 | 1 | 0 | 0 | 0 | 0 | 10 | 0.9 | 0 |
| Range Land | 0 | 8 | 0 | 0 | 1 | 1 | 10 | 0.8 | 0 |
| Bare land | 0 | 3 | 7 | 0 | 0 | 0 | 10 | 0.7 | 0 |
| Built Up | 0 | 1 | 1 | 8 | 0 | 0 | 10 | 0.8 | 0 |
| Bare Hill Surface | 0 | 3 | 2 | 0 | 5 | 0 | 10 | 0.5 | 0 |
| Waterbody | 0 | 0 | 1 | 0 | 0 | 9 | 10 | 0.9 | 0 |
| Total Producer | 9 | 16 | 11 | 8 | 6 | 10 | 60 | 0 | 0 |
| Producer Accuracy | 1 | 0.50 | 0.543 | 1 | 0.833333 | 0.9 | 0 | 0.766667 | 0 |
| Kappa Co-efficient | 0 | 0 | 0 | 0 | 0 | 0 | 0 | 0 | 0.72 |

$$\text{Overall Accuracy} = \frac{\text{Total Number of Correctly Classified Pixels in each Category}}{\text{Total Numer of Reference Pixels}} \text{ x } 100 \quad (7)$$

Total number of correctly classified pixels in each category = 9+8+7+8+5+9= 46

Total number of the reference pixels= 10+10+10+10+10= 60

$$\text{Overall Accuracy} = \frac{46}{60} \text{ x } 100 = 76.67\%$$

$$\text{Kappa coefficient} = \frac{(\text{TS x TCS}) - \sum (\text{Column Total x Row Total})}{\text{TS2} - \sum (\text{Column Total} - \text{Row Total})} \text{ x } 100 \quad (8)$$

Kappa coefficient =72%

The kappa coefficient is substantial (i.e very good)

#### 4.2.2.2 2020 Landsat 8 Accuracy Assessment

**Table 13: 2020 Landsat 8 Accuracy Assessment Table**

| | Vegetation | Range Land | Bare land | Built up | Bare Hill Surface | Waterbody | Total User | User Accuracy | Kappa Co-efficient |
|---|---|---|---|---|---|---|---|---|---|
| Vegetation | 8 | 2 | 0 | 0 | 0 | 0 | 10 | 0.8 | 0 |
| Range Land | 1 | 9 | 0 | 0 | 0 | 0 | 10 | 0.9 | 0 |
| Bare land | 0 | 2 | 7 | 0 | 1 | 0 | 10 | 0.7 | 0 |
| Built Up | 0 | 0 | 0 | 8 | 0 | 2 | 10 | 0.8 | 0 |
| Bare Hill Surface | 1 | 2 | 0 | 0 | 7 | 0 | 10 | 0.7 | 0 |
| Waterbody | 0 | 0 | 0 | 0 | 0 | 10 | 10 | 1 | 0 |
| Total Producer | 10 | 15 | 7 | 8 | 8 | 12 | 60 | 0 | 0 |
| Producer Accuracy | 0.8 | 0.6 | 1 | 1 | 0.875 | 0.833333 | 0 | 0.816667 | 0 |
| Kappa Co-efficient | 0 | 0 | 0 | 0 | 0 | 0 | 0 | 0 | 0.78 |

$$\text{Overall Accuracy} = \frac{\text{Total Number of Correctly Classified Pixels in each Category}}{\text{Total Numer of Reference Pixels}} \text{ x } 100 \quad (9)$$

$$\text{Overall Accuracy} = \frac{49}{60} \text{ x } 100 = 81.67\%$$

$$\text{Kappa coefficient} = \frac{(\text{TS x TCS}) - \sum (\text{Column Total x Row Total})}{\text{TS2} - \sum (\text{Column Total} - \text{Row Total})} \text{ x } 100 \quad (10)$$

Kappa coefficient =78%

The kappa coefficient is substantial (i.e. very good)

#### 4.2.2.3 2022 Landsat 8 Accuracy Assessment

**Table 14: 2022 Landsat 8 Accuracy Assessment Table**

| | Vegetation | Range Land | Bare land | Built up | Bare Hill Surface | Waterbody | Total User | User Accuracy | Kappa Co-efficient |
|---|---|---|---|---|---|---|---|---|---|
| Vegetation | 8 | 2 | 0 | 0 | 0 | 0 | 10 | **0.777778** | **0** |
| Range Land | 0 | 10 | 0 | 0 | 0 | 0 | 10 | **1** | **0** |
| Bare land | 0 | 0 | 9 | 0 | 1 | 0 | 10 | **0.9** | **0** |
| Built Up | 0 | 0 | 0 | 9 | 0 | 1 | 10 | **0.9** | **0** |
| Bare Hill Surface | 0 | 2 | 3 | 0 | 5 | 0 | 10 | **0.5** | **0** |
| Waterbody | 0 | 0 | 0 | 0 | 0 | 10 | 10 | **1** | **0** |
| Total Producer | 8 | 14 | 12 | 9 | 6 | 11 | 60 | **0** | **0** |
| Producer Accuracy | 1 | 0.714286 | 0.75 | 1 | 0.833333 | 0.909091 | 0 | **0.847458** | **0** |
| Kappa Co-efficient | 0 | 0 | 0 | 0 | 0 | 0 | 0 | **0** | **0.81677** |

$$\text{Overall Accuracy} = \frac{\text{Total Number of Correctly Classified Pixels in each Category}}{\text{Total Numer of Reference Pixels}} \text{ x } 100 \quad (11)$$

Total number of correctly classified pixels in each category = 8+10+9+9+5+10= 50

Total number of the reference pixels= 10+10+10+10+10= 60

$$\text{Overall Accuracy} = \frac{51}{60} \text{ x } 100 = 84.75\%$$

$$\text{Kappa coefficient} = \frac{(\text{TS x TCS}) - \sum(\text{Column Total x Row Total})}{\text{TS2} - \sum(\text{Column Total} - \text{Row Total})} \text{ x } 100 \quad (12)$$

Kappa coefficient = 81.67%

The kappa coefficient is substantial (i.e very good)

**Table 15:** 2018 Landsat 8 User Accuracy Percentage

| Class Name | User Accuracy Percentage |
|---|---|
| Vegetation | 90% |
| Rangeland | 80% |
| Bare land | 70% |
| Built up | 80% |
| Bare Hill Surface | 50% |
| Water Body | 90% |

**Table 16:** 2018 Landsat 8 Producer Accuracy Percentage

| Class Name | User Accuracy Percentage |
|---|---|
| Vegetation | 100% |
| Rangeland | 50% |
| Bare land | 53.53% |
| Built up | 100% |
| Bare Hill Surface | 83.33% |
| Water Body | 100% |

**Table 17:** 2020 Landsat 8 User Accuracy Percentage

| Class Name | User Accuracy Percentage |
|---|---|
| Vegetation | 80% |
| Rangeland | 90% |
| Bare land | 70% |
| Built up | 80% |
| Bare Hill Surface | 70% |
| Water Body | 100% |

**Table 18:** 2020 Landsat 8 Producer Accuracy Percentage

| Class Name | Producer Accuracy Percentage |
|---|---|
| Vegetation | 80% |
| Rangeland | 60% |
| Bare land | 100% |
| Built up | 100% |
| Bare Hill Surface | 87.5% |
| Water Body | 83.33% |

**Table 19:** 2022 Landsat 8 User Accuracy Percentage

| Class Name | User Accuracy Percentage |
|---|---|
| Vegetation | 77.8% |
| Rangeland | 100% |
| Bare land | 90% |
| Built up | 90% |
| Bare Hill Surface | 50% |
| Water Body | 100% |

**Table 20:** 2022 Landsat 8 Producer Accuracy Percentage

| Class Name | Producer Accuracy Percentage |
|---|---|
| Vegetation | 100% |
| Rangeland | 71.42% |
| Bare land | 75% |
| Built up | 100% |
| Bare Hill Surface | 83.33% |
| Water Body | 90.9% |

The Kappa coefficient provides a statistical measure of agreement between the classified map and the reference data, adjusting for the possibility of agreement occurring by chance. A value of 1 indicates perfect agreement, while 0 indicates no agreement beyond random chance. In this study, Kappa values ranged from 0.72 (substantial agreement) to 0.84 (almost perfect agreement), which confirms the reliability of the ANN classification in both Sentinel-2 and Landsat 8 datasets. Importantly, these values show that the classification results are not only accurate but also statistically robust, reducing the likelihood that the observed agreement is coincidental.

***Table 12. 2018 Landsat 8 Accuracy Assessment***

**Overall Accuracy**: 76.67%, Kappa Coefficient: 0.72 (substantial agreement)

**Observation:** Vegetation and waterbodies achieved high user accuracy (0.90), showing strong classification. On the contrary, bare hill surfaces had the lowest user accuracy (0.50), reflecting spectral confusion with bare land. This indicates that while ANN produced reliable results, distinguishing between spectrally similar classes remained a challenge in 2018.

***Table 13. 2020 Landsat 8 Accuracy Assessment***

**Overall Accuracy:** 81.67%, Kappa Coefficient: 0.78 (substantial agreement)

**Observation:** Classification performance improved compared to 2018. Vegetation, built-up areas, and waterbodies maintained high accuracies (≥ 0.80 user accuracy), while bare land and bare hill surfaces still showed moderate confusion. This suggests that the ANN classifier adapted better to the 2020 imagery but continued to struggle with classes of similar spectral properties.

***Table 14. 2022 Landsat 8 Accuracy Assessment***

**Overall Accuracy:** 84.75%

**Kappa Coefficient:** 0.82 (almost perfect agreement)

Observation: Accuracy reached its highest level in 2022, with vegetation, built-up areas, and waterbodies showing excellent classification (≥ 0.90 user accuracy). However, bare hill surfaces again recorded the lowest accuracy (0.50), consistent with earlier years. This indicates steady improvements in overall classification reliability, but also highlights persistent challenges in distinguishing spectrally similar land cover types.

The classified imageries reveal noticeable temporal variations in feature distribution. For instance, some years showed higher proportions of built-up areas and vegetation, reflecting ongoing urban expansion and reforestation/greening efforts within Abuja and its environs. In contrast, imageries with larger proportions of bare hill surfaces likely correspond to natural geomorphological exposure or reduced vegetation cover during drier seasons, making rocky surfaces more prominent. These variations underscore the combined influence of urbanization,

seasonal vegetation dynamics, and environmental conditions on land cover distribution. Across all three years, Sentinel-2 consistently achieved higher accuracy than Landsat 8. This performance difference can be attributed to several factors:

**Spatial Resolution:** Sentinel-2 provides 10–20 m resolution in key visible and near-infrared bands, compared to Landsat 8's 30 m resolution, allowing Sentinel-2 to capture finer details of urban and vegetation patterns.

**Spectral Bands**: Sentinel-2 has 13 spectral bands, including specialized red-edge bands useful for vegetation monitoring, while Landsat 8 has 11 bands. The additional spectral information enhances Sentinel-2's ability to distinguish between similar classes.

**Temporal Resolution**: Sentinel-2 revisits every 5 days (with both satellites), compared to Landsat 8's 16-day revisit, meaning Sentinel-2 can provide more cloud-free imagery options and capture seasonal dynamics more effectively.

These advantages explain why Sentinel-2 classification accuracy improved steadily from 2018 to 2022, reaching an overall accuracy of 86.7% with a Kappa coefficient of 0.84, compared to Landsat 8's 84.75% and 0.82 in the same period. While both datasets performed well, Sentinel-2's higher spatial and spectral resolution made it better suited for capturing the heterogeneous land cover of Abuja.

## 4.3 Change Detection Analysis

### 4.3.1 Change Detection Analysis on the Sentinel Imageries

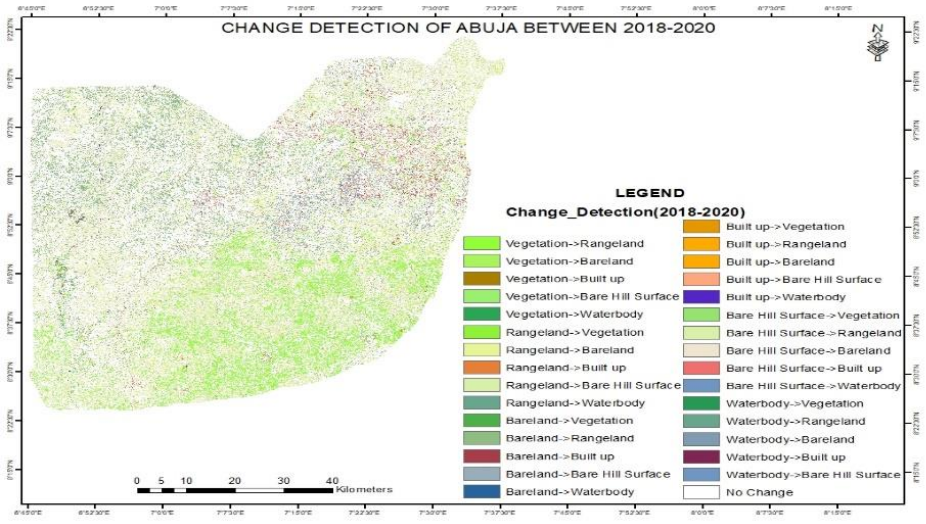


**Fig. 7: Change Detection for Abuja Between 2018 and 2020**

The change detection analysis highlights both stability and significant transitions in land cover. For example, the conversion of bare hill surface to bare land (5.63% between 2018 and 2020) may indicate soil erosion, land degradation, or quarrying activities, which expose soils previously covered by rocky or semi-vegetated surfaces. Meanwhile, increases in built-up areas at the expense of vegetation and rangeland strongly point to urbanization and infrastructure development in Abuja.

Between 2020 and 2022, the substantial shifts such as bare land to rangeland (6.7%) suggest natural vegetation regrowth or agricultural reclamation of previously exposed areas, possibly linked to land management practices. Conversely, reductions in vegetation and increases in bare surfaces may also reflect climate variability, particularly droughts or seasonal rainfall fluctuations, which can temporarily reduce vegetative cover.

These findings illustrate that the observed changes are not random but are strongly connected to human activities (urban growth, farming, quarrying) and natural/environmental processes (erosion, drought, seasonal cycles) shaping the Abuja landscape.

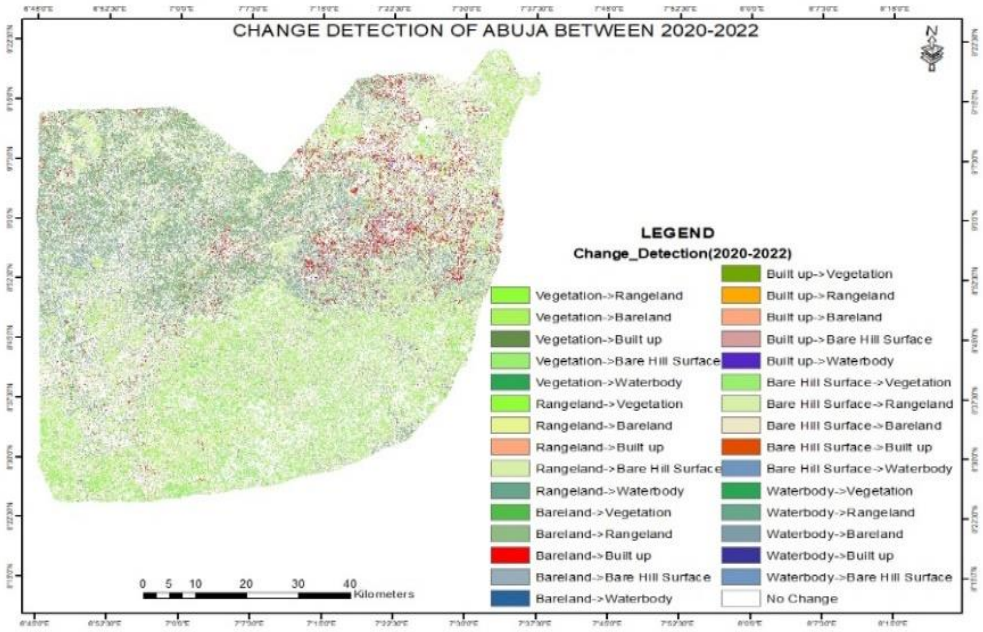


**Fig. 8: Change Detection for Abuja between 2020 and 2022**

**Table 21: Change Detection Analysis for the Sentinel 2 Data between 2018 and 2020**

| Class_name | Area Change | Change in % |
|---|---|---|
| Vegetation->Rangeland | 1622319 | 3.6909927 |
| Vegetation->Bareland | 427333 | 0.972239728 |
| Vegetation->Built up | 595200 | 1.354159604 |
| Vegetation->Bare Hill Surface | 826687 | 1.880823489 |
| Vegetation->Waterbody | 492584 | 1.12069448 |
| Rangeland->Vegetation | 506673 | 1.152748839 |
| Rangeland->Bareland | 1040175 | 2.366537242 |
| Rangeland->Built up | 668671 | 1.521315956 |
| Rangeland->Bare Hill Surface | 726202 | 1.652206675 |
| Rangeland->Waterbody | 717516 | 1.632444863 |
| Bareland->Vegetation | 950497 | 2.162507798 |
| Bareland->Rangeland | 953785 | 2.169988438 |
| Bareland->Built up | 873154 | 1.986542129 |
| Bareland->Bare Hill Surface | 1160011 | 2.639180169 |
| Bareland->Waterbody | 1275294 | 2.901464413 |
| Built up->Vegetation | 1040835 | 2.36803883 |
| Built up->Rangeland | 1475272 | 3.356441108 |
| Built up->Bareland | 1250222 | 2.844422259 |
| Built up->Bare Hill Surface | 1396567 | 3.177376707 |
| Built up->Waterbody | 1452035 | 3.303573826 |
| Bare Hill Surface->Vegetation | 1758369 | 4.000524646 |
| Bare Hill Surface->Rangeland | 1732449 | 3.941553179 |
| Bare Hill Surface->Bareland | 2476859 | 5.635185489 |
| Bare Hill Surface->Built up | 2070197 | 4.709975051 |
| Bare Hill Surface->Waterbody | 2221790 | 5.0548694 |
| Waterbody->Vegetation | 1614159 | 3.672427609 |
| Waterbody->Rangeland | 1955420 | 4.448842025 |
| Waterbody->Bareland | 2326022 | 5.292011141 |
| Waterbody->Built up | 1318365 | 2.999456698 |
| Waterbody->Bare Hill Surface | 1086003 | 2.470802071 |
| No Change | 5942795 | 13.52065344 |
| SUM | 43953460 | 100 |

**Table 22: Change Detection Analysis for the Sentinel 2 Data between 2020 and 2022**

| Class_name | Area Change | Change in % |
|---|---|---|
| Vegetation->Rangeland | 101782 | 0.138334438 |
| Vegetation->Bareland | 82479 | 0.112099252 |
| Vegetation->Built up | 132616 | 0.180241691 |
| Vegetation->Bare Hill Surface | 250552 | 0.34053143 |
| Vegetation->Waterbody | 192810 | 0.262052848 |
| Rangeland->Vegetation | 554277 | 0.753331602 |
| Rangeland->Bareland | 917076 | 1.246420711 |
| Rangeland->Built up | 1457199 | 1.980515261 |
| Rangeland->Bare Hill Surface | 2335486 | 3.174216881 |
| Rangeland->Waterbody | 1232974 | 1.675765509 |
| Bareland->Vegetation | 2127752 | 2.891880455 |
| Bareland->Rangeland | 5009162 | 6.808076169 |
| Bareland->Built up | 3257573 | 4.427448166 |
| Bareland->Bare Hill Surface | 3401209 | 4.622667412 |
| Bareland->Waterbody | 2912760 | 3.958804276 |
| Built up->Vegetation | 3349672 | 4.552622199 |
| Built up->Rangeland | 2969554 | 4.035994408 |
| Built up->Bareland | 3216965 | 4.372256828 |
| Built up->Bare Hill Surface | 2987580 | 4.060493991 |
| Built up->Waterbody | 2592176 | 3.523090619 |
| Bare Hill Surface->Vegetation | 3625593 | 4.927633266 |
| Bare Hill Surface->Rangeland | 2868700 | 3.898921238 |
| Bare Hill Surface->Bareland | 3844461 | 5.225102186 |
| Bare Hill Surface->Built up | 2905163 | 3.948479005 |
| Bare Hill Surface->Waterbody | 3268630 | 4.442476009 |
| Waterbody->Vegetation | 2815371 | 3.826440473 |
| Waterbody->Rangeland | 2801812 | 3.8080121 |
| Waterbody->Bareland | 3163670 | 4.299822273 |
| Waterbody->Built up | 2183066 | 2.967059083 |
| Waterbody->Bare Hill Surface | 739545 | 1.005133931 |
| No Change | 6279097 | 8.534076289 |
| SUM | 73576762 | 100 |

Preliminary observations from the change detection tables indicate that the built-up areas have been continuously increasing, and the vegetation and rangeland have been continuously decreasing during the period of the research, which can be explained by the high urbanization rate in Abuja. For instance, the 2018–2020 Sentinel-2 data show notable transitions from bare hill surfaces to bare land (≈5.6%) and from built-up to vegetation or rangeland (≈2–3%), while the 2020–2022 results indicate a sharper increase in bare land to rangeland (≈6.8%) and built-up expansion into adjacent classes (≈4–5%). Indicators of such trends, e.g., the steady increase in the built-up area or slow decline in the rangelands, would show the dynamics of the land cover than year-to-year comparisons.

### 4.3.2 Change Detection Analysis on the Landsat Imageries

**Table 15: Change Detection Analysis for the Sentinel 2 Data between 2018 and 2020**

| Class_name | Area Change | Change in % |
|---|---|---|
| Vegetation->Rangeland | 1851 | 0.04531029 |
| Vegetation->Bareland | 1558 | 0.03813799 |
| Vegetation->Builtup | 2371 | 0.05803927 |
| Vegetation->Bare Hill Surface | 4144 | 0.10144021 |
| Vegetation->Water body | 3670 | 0.08983725 |
| Rangeland->Vegetation | 29355 | 0.71857563 |
| Rangeland->Bareland | 56490 | 1.38280828 |
| Rangeland->Builtup | 81520 | 1.99551303 |
| Rangeland->Bare Hill Surface | 195428 | 4.78384594 |
| Rangeland->Water body | 43053 | 1.05388644 |
| Bareland->Vegetation | 149961 | 3.67086764 |
| Bareland->Rangeland | 58382 | 1.4291222 |
| Bareland->Builtup | 143844 | 3.52113073 |
| Bareland->Bare Hill Surface | 94566 | 2.31486366 |
| Bareland->Water body | 113719 | 2.78370641 |
| Builtup->Vegetation | 144113 | 3.52771553 |
| Builtup->Rangeland | 141977 | 3.47542878 |
| Builtup->Bareland | 171384 | 4.1952773 |
| Builtup->Bare Hill Surface | 128972 | 3.15708178 |
| Builtup->Water body | 148090 | 3.62506778 |
| Bare Hill Surface->Vegetation | 216656 | 5.30348223 |
| Bare Hill Surface->Rangeland | 206696 | 5.05967323 |
| Bare Hill Surface->Bareland | 312307 | 7.64490541 |
| Bare Hill Surface->Builtup | 162073 | 3.96735505 |
| Bare Hill Surface->Water body | 254292 | 6.22476693 |
| Water body->Vegetation | 197995 | 4.84668306 |
| Water body->Rangeland | 151430 | 3.70682702 |
| Water body->Bareland | 263344 | 6.44634917 |
| Water body->Builtup | 105297 | 2.57754583 |
| Water body->Bare Hill Surface | 80568 | 1.9722092 |
| No Change | 420059 | 10.2825467 |
| SUM | 4085165 | 100 |

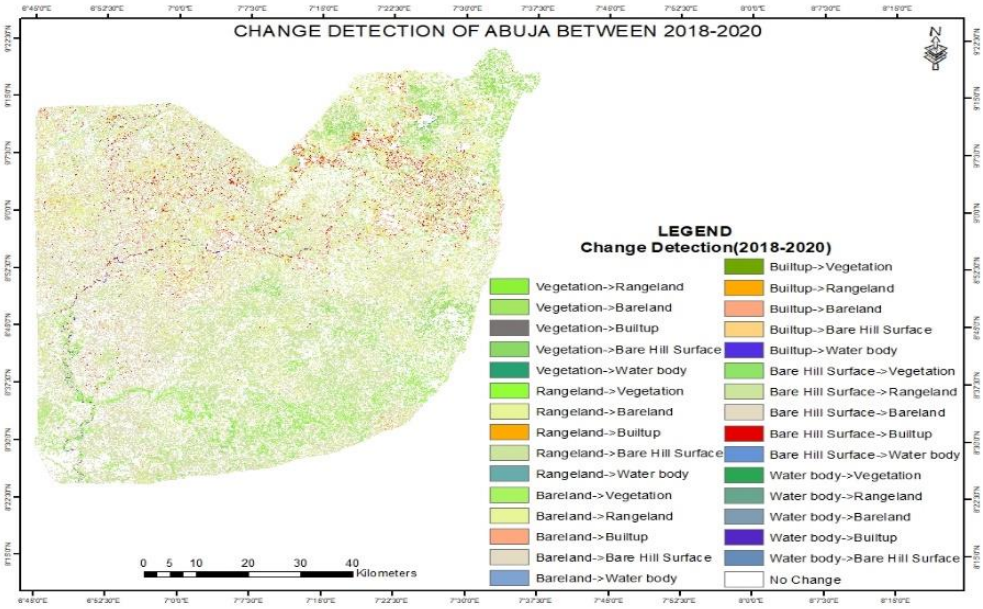


**Fig. 9:** **Change Detection for Abuja between 2018 and 2020**

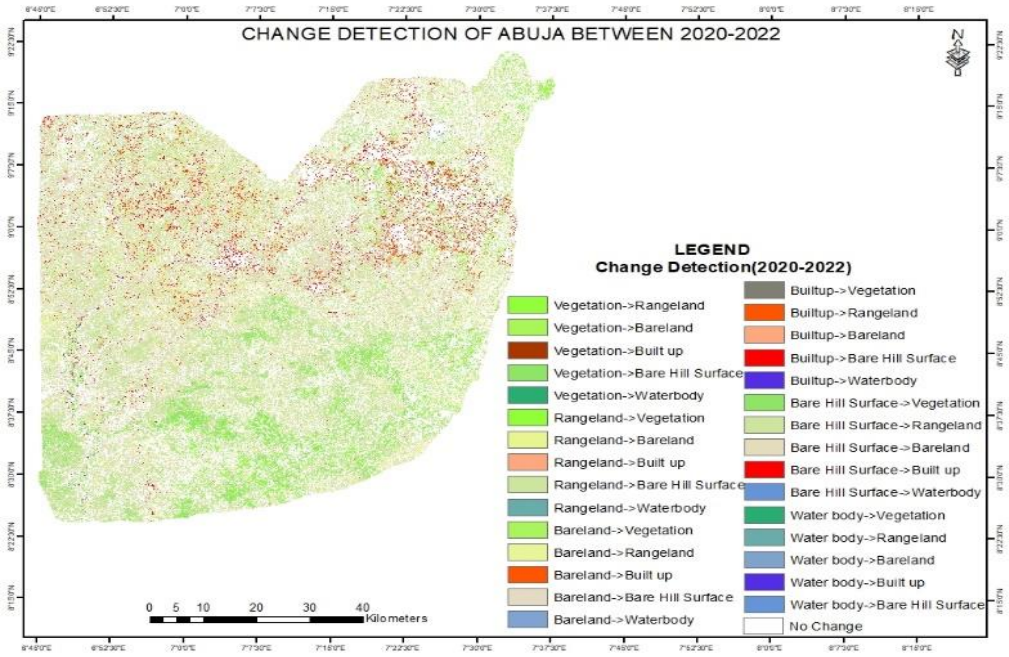


**Fig. 10:** **Change Detection for Abuja between 2020 and 2022**

**Table 16: Change Detection for Abuja between 2020 and 2022**

| Class_name | Area Change | Change in % |
|---|---|---|
| Vegetation->Rangeland | 5269 | 0.10777297 |
| Vegetation->Bareland | 2494 | 0.05101268 |
| Vegetation->Built up | 3119 | 0.06379653 |
| Vegetation->Bare Hill Surface | 7428 | 0.1519335 |
| Vegetation->Waterbody | 4617 | 0.09443686 |
| Rangeland->Vegetation | 6761 | 0.13829058 |
| Rangeland->Bareland | 16430 | 0.33606185 |
| Rangeland->Built up | 27350 | 0.55942128 |
| Rangeland->Bare Hill Surface | 40659 | 0.83164569 |
| Rangeland->Waterbody | 36626 | 0.74915407 |
| Bareland->Vegetation | 80516 | 1.64688715 |
| Bareland->Rangeland | 129177 | 2.64220704 |
| Bareland->Built up | 170842 | 3.49442962 |
| Bareland->Bare Hill Surface | 211155 | 4.31899817 |
| Bareland->Waterbody | 214118 | 4.37960385 |
| Builtup->Vegetation | 214547 | 4.38837868 |
| Builtup->Rangeland | 248066 | 5.07398167 |
| Builtup->Bareland | 242937 | 4.96907229 |
| Builtup->Bare Hill Surface | 263013 | 5.37971001 |
| Builtup->Waterbody | 241946 | 4.94880221 |
| Bare Hill Surface->Vegetation | 354289 | 7.24668392 |
| Bare Hill Surface->Rangeland | 408653 | 8.35865388 |
| Bare Hill Surface->Bareland | 316730 | 6.47844612 |
| Bare Hill Surface->Built up | 292295 | 5.97864872 |
| Bare Hill Surface->Waterbody | 254591 | 5.20744507 |
| Water body->Vegetation | 221185 | 4.5241534 |
| Water body->Rangeland | 203444 | 4.16127614 |
| Water body->Bareland | 207122 | 4.23650654 |
| Water body->Built up | 119877 | 2.45198335 |
| Water body->Bare Hill Surface | 63216 | 1.29303018 |
| No Change | 280509 | 5.73757599 |
| Sum | 4888981 | 100 |

## 4.4 Result Analysis

The result of the operation carried out in this study include the LULC (Land Use and Land Cover) map of the data collected, Landsat 8 and Sentinel data, for year 2018, 2020, 2022, which was produced using ANN (Artificial Neural Network) classification algorithm. It also includes the accuracy assessment of the classified imageries using the confusion matrix, and the change detection analysis of the classified imageries.

To produce LULC map for the Landsat 8 and Sentinel 2 imageries collected, the features in the imageries were divided into six classes, vegetation, rangeland, bare land, built up, bare hill surface and water body. The result of the classified imageries shows that there is more built up and vegetation in some imageries, and there is barer hill surface in some classified imageries. This is dependent on the year and accuracy of the classified imagery.

Table 21, 22, 23 and 24 shows the percentage of changes from one feature class to the other. Table 21 and 22 shows the percentage of change for the classified sentinel 2 data between 2018 and 2020, and 2020 and 2022 respectively. The change detection analysis of the 2018 to 2020 sentinel data shows that there is higher percentage of no changes of the feature classes, with the percentage value of 13%. The highest percentage change between 2018 and 2020 is the bare hill surface to bare land, with a percentage of 5.63%, while the lowest is vegetation to rangeland with the percentage of 0.9%. For the change detection analysis between 2020 and 2022 of the sentinel data, the percentage of changes shows that there is significant change between the years 2020 to 2022. The most significant change is bare land to range land with the percentage of is 6.7% while the lowest change is vegetation to rangeland, with the percentage value 0.05%.

The conversion of bare hill surfaces to bare land (≈5% between 2018–2020) is significant from a land management perspective. It suggests environmental degradation processes such as soil erosion, deforestation, or quarrying activities that expose underlying soils. This shift highlights potential sustainability concerns, as continuous loss of protective vegetation and surface cover can increase erosion risk and reduce land productivity. Similarly, the consistent transition of vegetation and rangeland into built-up areas across both Sentinel-2 and Landsat 8 datasets reflects rapid urban expansion in Abuja. This pattern aligns with Abuja's role as Nigeria's capital city, where infrastructure development and housing demands are steadily increasing. While this indicates economic growth, it also raises challenges related to loss of agricultural land, biodiversity decline, and increased urban heat island effects.

The period between 2018 and 2020 showed notable increases in conversions such as bare hill surfaces to bare land and rangeland to built-up areas, suggesting intensified human disturbance and land development. This may correspond with infrastructure projects and population growth during that time. Between 2020 and 2022, however, more substantial changes were observed in the bare land to rangeland category, indicating vegetation regrowth or agricultural reclamation of previously degraded land. This could reflect shifts in land management practices, post-development rehabilitation, or even the influence of government policies promoting reforestation and agricultural use. Notably, built-up expansion continued in both periods, but the simultaneous increase in rangeland from bare land suggests that while urbanization pressures persist, land recovery and adaptation efforts are

also occurring. This dynamic underscores Abuja's dual challenges: managing urban growth while ensuring environmental resilience.

For the Landsat 8 data, the change detection analysis between 2018 and 2020 shows that the percentage of no change is higher than the percentage of changes that occur, which is similar to the result obtained for the sentinel 2 data. The percentage of no change is 10.3%. The highest percentage change is bare hill surface to bare land, and the lowest change is vegetation to rangeland change. The change detection between 2020 and 2022 shows that there is more significant change between these years. The highest percentage change is bare hill surface to rangeland, with the percentage value of 8.3% and the lowest percentage change is vegetation to bare land, with the value 0.

The observed land cover changes provide important insights for urban planning, land management, and conservation in Abuja. The steady increase in built-up areas, often at the expense of vegetation and rangeland, reflects the city's rapid urbanization and growing population. These findings underscore the need for strategic planning to manage urban sprawl, ensure adequate infrastructure, and balance development with the preservation of agricultural and ecological resources. At the same time, the conversion of vegetation into bare land or bare hill surface suggests deforestation, erosion, and land degradation, pointing to the importance of environmental conservation efforts such as reforestation programs, erosion control, and sustainable land management practices.

Beyond environmental implications, the results also connect to socio-economic trends in the region. The conversion of bare land back to rangeland, especially between 2020 and 2022, may reflect natural regrowth or agricultural reclamation, supporting food security and rural livelihoods. However, continued urban expansion into rangeland increases competition for land between residential and agricultural uses, with potential impacts on rural communities and land values. Together, these patterns highlight that land cover change is not random but shaped by the interaction of human activities, policy decisions, and natural processes. As such, change detection analysis serves not only as a technical assessment but as a decision-support tool for policymakers, planners, and environmental managers working to balance urban growth with sustainability and resilience.

The higher percentage of change in certain transitions, e.g. bare hill surface to bare land, has significant implications. These changes imply that the processes of environmental degradation (e.g., erosion, quarrying, or loss of vegetation) may decrease the productivity of land and make it more ecologically vulnerable. Bare land to rangeland increases on the other hand indicate recovery of land or agricultural reclamation, which underlines landscape resilience. In the case of urban planning and land management, such shifts indicate where efforts must be

undertaken to counter the urban growth due erosion, sustainable farming, or balancing the urban growth with conservation. Although more complex deep learning networks like U-Net, CNNs, RNNs and more complex networks like ResNet are indeed more suitable to support high-dimensional data and contextual spatial relationships, ANN was used in this study due to two reasons. Firstly, ANNs are computationally simpler and can be instantiated using comparatively small quantities of hardware than deep learning models, and are therefore more readily applicable in resource-limited settings. Second, ANN has continued to be a popular baseline technique in remote sensing research and provides a benchmark against which more recent classifiers can be evaluated. The findings here with accuracies always exceeding 80 percent illustrate that ANN can still give credible classifications with other advanced architectures, though this can be done better. Even though Support Vector Machines (SVM) can be more effective in terms of accuracy of classifying data, especially when the dataset consists of Sentinel-2 and Landsat 8, it is noteworthy to compare ANN with other models. The reason is that ANN has some other modeling perspective that has the ability to describe non-linear relationships within the data and it can be used as a benchmark with which to compare. This study illustrates the advantages and weaknesses of ANN in this regard, which will help to gain a more holistic picture of the performance of the classifier in the context of LULC mapping [43],[44].

## 5 DISCUSSIONS

Over the past ten years, due to its significance on a worldwide level, the necessity to depict, examine, and oversee land cover has grown crucial. The remarkable advancements in remote sensing technology have greatly advanced the field of land cover mapping [24].

The objective of this study was to assess the effectiveness of Artificial Neural Network (ANN) for feature detection in Sentinel-2 and Landsat 8 satellite imagery. This study aimed to evaluate the performance of ANN in producing accurate land cover classifications and to compare the results between the two satellite datasets. In a comparative study by [25], the effectiveness of Support Vector Machine (SVM), Artificial Neural Network (ANN), Maximum Likelihood Classification (MLC), Minimum Distance (MD), and Mahalanobis (MH) algorithms was evaluated for creating Land Use and Land Cover (LULC) maps using Sentinel 2 and Landsat 8 data, with SVM achieving the highest accuracy of 94%, surpassing alternative methods and demonstrating slightly better performance with Sentinel 2 data over Landsat 8, while MD and MLC exhibited lower accuracies of 80.85% and 74.68% for both datasets.

To achieve this goal, this study conducted an assessment of the ANN algorithm by using Sentinel-2 and Landsat 8 data for feature detection. The data collected included imagery from the years 2018, 2020, and 2022. The primary focus was on the production of Land Use and Land Cover (LULC) maps using the ANN classification algorithm.

This study employs ANNs to classify six distinct feature classes: vegetation, rangeland, bare land, built-up areas, bare hill surfaces, and water bodies. The integration of ANNs enables the accurate classification of these features, providing a comprehensive understanding of land use and land cover (LULC) patterns. The results of the classified imageries revealed the varying distribution of the feature classes across different imageries, which depended on the year and accuracy of the classified imagery. Some imageries showed higher proportions of built-up areas and vegetation, while others displayed more bare hill surfaces. These variations highlighted the temporal changes and the impact of classification accuracy on the final LULC maps.

The accuracy assessment carried out in the study demonstrated the performance of the ANN algorithm for feature detection in Sentinel-2 and Landsat 8 data. The classified imageries of Sentinel-2 data consistently achieved higher accuracy compared to Landsat 8 data for the three years evaluated. The overall accuracy values were 80.33%, 83.33%, and 86.67% for Sentinel-2 and 78.33%, 81.45%, and 84.75% for Landsat 8. The Kappa coefficient analysis further confirmed the higher accuracy of Sentinel-2 data compared to Landsat 8. In a study by [26], the effectiveness of algorithms including Artificial Neural Network, Support Vector Machine, and Genetic Algorithm was explored to develop an efficient and intelligent information retrieval model. Experimental results highlighted that the neural network, whether used in conjunction with the Genetic Algorithm or independently, showcased enhanced performance compared to other methods.

This study has also found that the findings are consistent with the results of larger studies conducted in the field of remote sensing, in which supervised classifiers have always been demonstrated to provide increased accuracy over unsupervised methods [24]. The Support Vector machines (SVM) are known to be the most accurate in comparative tests on the various classifiers, although the Artificial Neural Networks (ANN) are also a competitor and are always able to win over the traditional ones, which include Maximum Likelihood Classification (MLC) and Minimum Distance (MD) [25]. This can be seen in the current work where ANN was able to generate consistent classifications in both the Sentinel-2 and Landsat 8 datasets, with the Sentinel-2 showing the highest accuracies. The other studies have also indicated that ANNs are also efficient particularly when they are used together with optimization techniques like Genetic Algorithms thus improving their classification capabilities even better [26]. Although this paper used ANN as a single classifier, the

high performance, particularly using Sentinel-2 images, can support that ANNs are highly applicable in land use and land cover assessment and also to compete favorably with the rest of the sophisticated machine learning algorithms.

Furthermore, this study examined the change detection analysis of the classified imageries. The percentage of changes between different feature classes was analyzed, providing insights into the dynamics of land cover changes over time. The results showed that there were significant changes observed between the years 2018 and 2020, as well as between 2020 and 2022, for both Sentinel-2 and Landsat 8 data. These changes varied across different feature classes, with some experiencing higher rates of change compared to others.

This study highlights that both Sentinel-2 and Landsat 8 datasets exhibit considerable change in feature classes, with variations in the rates of change among different classes. These findings emphasize the need for precise and accurate feature detection techniques, as they form the foundation for reliable change detection and monitoring of land cover transformations

## 6 SUMMARY

This study aimed to assess the effectiveness of the Artificial Neural Network (ANN) for feature detection in Sentinel-2 and Landsat 8 satellite imagery. It sought to evaluate the accuracy of land cover classifications using ANN and compare outcomes between the two datasets. This involved assessing the ANN algorithm with imagery from 2018, 2020, and 2022, primarily focusing on generating Land Use and Land Cover (LULC) maps categorized into six classes.

The classified imagery results unveiled variations in feature distribution across different images, influenced by the year and classification accuracy. Sentinel-2 consistently exhibited higher accuracy compared to Landsat 8, with overall accuracy values ranging from 80.33% to 86.67% for Sentinel-2 and 78.33% to 84.75% for Landsat 8. The Kappa coefficient analysis confirmed Sentinel-2's superior accuracy.

Additionally, this study analyzed changes between feature classes over time through change detection analysis. This revealed significant changes between the years 2018 and 2020, as well as 2020 and 2022, for both datasets. These changes varied among feature classes, indicating dynamic shifts in land cover.

## 6.1 Conclusion

In conclusion, the assessment of the use of Artificial Neural Network for feature detection in Sentinel-2 and Landsat 8 imagery highlighted the effectiveness of the ANN algorithm in producing accurate land cover classifications. This study demonstrated the superiority of Sentinel-2 data in terms of classification accuracy compared to Landsat 8 data. The change detection analysis further emphasized the temporal dynamics of land cover changes. These findings contribute to the understanding of the capabilities and limitations of ANN for feature detection and provide valuable insights for remote sensing applications.

# 7 REFERENCES


[1] L. K. Gupta, "Dstl Satellite Imagery Feature Detection," 11 December 2020. [Online]. Available: https://medium.com/thecyphy/dstl-satellite-imagery-feature-detection-f186048de52e.

[2] "Significance of Land Use / Land Cover (LULC) Maps," 2017. [Online]. Available: https://www.satpalda.com/blogs/significance-of-land-use-land-cover-lulc-maps.

[3] M. M. Yemane, "An Assessment of Changes in Land Use/Cover Patterns," 2003. [Online]. Available: https://citeseerx.ist.psu.edu/document?repid=rep1&type=pdf&doi=6b5fbc04c72faa66b7c6753691dc7c3d96f1f177.

[4] K. E. M. ,. M. H. V. E. H. H. R. K. L. L. C. P. J. ,. H. A. R. Tobias, "Challenges and opportunities in mapping land use intensity globally," ELSEVIER, OCTOBER 2013.

[5] A. S. K. G. Himan, "Flood Detection and Susceptibility Mapping Using Sentinel-1 Remote Sensing Data and a Machine Learning Approach: Hybrid Intelligence of Bagging Ensemble Based on K-Nearest Neighbor Classifier," Special Issue Remote Sensing of Water Resources Monitoring, Parametrization and Modeling, 2020.

[6] J. M. S. S. H. Al-Doski, "Image classification in remote sensing. J. Environ. Earth Sci," Journal of Environment and Earth Science, pp. 3, 10, 2013.

[7] O. K. A. Rozenstein, "Comparison of methods for land-use classification incorporating remote sensing and GIS inputs.," Applied Geography, pp. 533-544, 2013.

[8] F. H. Al-Ahmadi, "Comparison of four classification methods to extract land use and land cover from raw satellite images," Earth, pp. 20, 167–191, 2009.

[9] L. N. Kantakumar, "Multi-temporal land use classification using hybrid approach," The Egyptian Journal of Remote Sensing and Space Science, pp. 18, 289–295., 2015.

[10] S. M. S. T. M. P. H. K. Yousefi, "Comparison of different algorithms for land use mapping in dry climate using satellite images: A case study of the Central regions of Iran," International Desert of Research Desert, pp. 20, 1-10, 2015.

[11] S. P. L. R. T. Bett, "Monitoring of urban sprawl using minimum distance supervised classification South Africa," Asia Life Science, pp. 9, 245–261, 2013.

[12] B. R. S. K. Rimal, "Comparing Support Vector Machines and Maximum Likelihood Classifiers for Mapping of," Journal of the Indian Society of Remote Sensing, pp. 48, 71–79., 2020.

[13] C. Zhang, I. Sargent, X. Pan, H. Li, A. Gardiner, J. Hare and P. Atkinson, "An object-based convolutional neural network (OCNN)," Remote Sensing of Environment, pp. 216, 57–70, 2018.

[14] P. Teluguntla, P. Thenkabail, A. Oliphant, J. Xiong, M. Gumma, R. Congalton, K. Yadav and Huete, "A 30-m landsat-derived cropland extent product of Australia and China using random forest machine learning algorithm on Google Earth Engine cloud computing platform," ISPRS Journal of Photogrammetry and Remote Sensing, pp. 216, 57–70, 2018.

[15] S. B. N. O. I. A. Martins, "Support vector machine algorithm optimal parameterization for change detection mapping in Funil Hydroelectric Reservoir (Rio de Janeiro State, Brazil)," Modeling Earth Systems and Environment, pp. 2, 138, 2016.

[16] K. Bahadur, "Improving Landsat and IRS Image Classification: Evaluation of Unsupervised and Supervised Classification through Band Ratios and DEM in a Mountainous Landscape in Nepal," Ecological Status and Change by Remote Sensing, pp. 1, 1257–1272., 2009.

[17] M. P. R. C. K. K. Boori, " Supervised and unsupervised classification for obtaining land use/cover classes from hyperspectral and multi-spectral imagery.," in In Proceedings

of the Sixth International Conference on Remote Sensing and Geoinformation of the Environment, Cyprus, 2018.

[18] H. Shahabi, A. Shirzadi, K. Ghaderi, E. Omidvar, N. Al-Ansari, J. Clague, M. Geertsema, K. Khosravi, A. Amini and B. S., "Flood detection and susceptibility mapping using sentinel-1 remote sensing data and a machine learning approach: Hybrid," Remote Sensing of Water Resources Monitoring, Parametrization and Modeling, pp. 12, 266, 2020.

[19] D. F. S. D. M. Duro, "A comparison of pixel-based and object-based image analysis with selected machine learning algorithms for the classification of agricultural landscapes using SPOT-5 HRG imagery," Remote Sensing of Environment, p. 259–272, 2012.

[20] L. L. M. M. X. C. L. D. P. L. Y. Ma, "A review of supervised object-based land-cover image classification.," ISPRS Journal of Photogrammetry and Remote Sensing, pp. 130, 277–293, 2017.

[21] Ahmadian, "Hydrogeological and Geomechanical Evaluation," IEEE Transactions on Geoscience and Remote Sensing, 2016.

[22] J. C. A. L. X. C. L. C. X. C. C. H. e. a. Chen, "Global Land Cover Mapping at 30m Resolution: A POK-based Operational Approach.”," ISPRS Journal of Photogrammetry andRemote Sensing, p. 7–27, 2015.

[23] M. U. D. B. S. C. O. C. V. F. F. G. B. H. C. I. P. L. a. P. M. Drusch, "Sentinel-2: ESA’s Optical High-Resolution Mission for GMES Operational Services," Remote Sensing of Environment 120, p. 25–36, 2012.

[24] M. G. S. S. Khatami, "A meta-analysis of remote sensing research on supervised pixel-based land covermage classification processes: General guidelines for," Remote Sens. Environ, p. 89–100., 2016.

[25] M. B. A. Kissinger, "Comparative Study of Some Supervised Machine Learning Algorithms," Saudi Journal of Engineering and Technology, pp. 2415-6264, 2020.

[26] L. Ghayour, A. Neshat, S. Paryani, H. Shahabi, A. Shirzadi, W. Chen, N. Al-Ansari, M. Geertsema, M. Pourmehdi Amiri and M. Gholamnia, "Performance Evaluation of Sentinel-2 and Landsat 8 OLI Data for Land Cover/Use Classification Using a Comparison between Machine Learning Algorithms," 2021.

[27] R. Khatami, G. Mountrakis, and S. V. Stehman, “A meta-analysis of remote sensing research on supervised pixel-based landcover image classification processes: General guidelines for practitioners and future research,” Remote Sensing of Environment, vol. 177, pp. 89–100, May 2016, doi: 10.1016/j.rse.2016.02.028.

[28] N. Gorelick, M. Hancher, M. Dixon, S. Ilyushchenko, D. Thau, and R. Moore, “Google Earth Engine: Planetary-scale geospatial analysis for everyone,” Remote Sensing of Environment, vol. 202, pp. 18–27, Dec. 2017, doi: 10.1016/j.rse.2017.06.031.

[29] G. M. Foody, “Status of land cover classification accuracy assessment,” Remote Sensing of Environment, vol. 80, no. 1, pp. 185–201, Apr. 2002, doi: 10.1016/s0034-4257(01)00295-4.

[30] M. Herold, H. Couclelis, and K. C. Clarke, “The role of spatial metrics in the analysis and modeling of urban land use change,” Computers, Environment and Urban Systems, vol. 29, no. 4, pp. 369–399, July 2005, doi: 10.1016/j.compenvurbsys.2003.12.001.

[31] C. Giri, Z. Zhu, and B. Reed, “A comparative analysis of the Global Land Cover 2000 and MODIS land cover data sets,” Remote Sensing of Environment, vol. 94, no. 1, pp. 123–132, Jan. 2005, doi: 10.1016/j.rse.2004.09.005.

[32] G. M. Foody and A. Mathur, “A relative evaluation of multiclass image classification by support vector machines,” IEEE Trans. Geosci. Remote Sensing, vol. 42, no. 6, pp. 1335–1343, June 2004, doi: 10.1109/tgrs.2004.827257.

[33] M. Belgiu and L. Drăguţ, “Random forest in remote sensing: A review of applications and future directions,” ISPRS Journal of Photogrammetry and Remote Sensing, vol. 114, pp. 24–31, Apr. 2016, doi: 10.1016/j.isprsjprs.2016.01.011.

[34] D. Lu and Q. Weng, “A survey of image classification methods and techniques for improving classification performance,” International Journal of Remote Sensing, vol. 28, no. 5, pp. 823–870, Mar. 2007, doi: 10.1080/01431160600746456.

[35] C. Zhang et al., “An object-based convolutional neural network (OCNN) for urban land use classification,” Remote Sensing of Environment, vol. 216, pp. 57–70, Oct. 2018, doi: 10.1016/j.rse.2018.06.034.

[36] L. Ma, Y. Liu, X. Zhang, Y. Ye, G. Yin, and B. A. Johnson, “Deep learning in remote sensing applications: A meta-analysis and review,” ISPRS Journal of Photogrammetry and Remote Sensing, vol. 152, pp. 166–177, June 2019, doi: 10.1016/j.isprsjprs.2019.04.015.

[37] M. Drusch et al., “Sentinel-2: ESA’s Optical High-Resolution Mission for GMES Operational Services,” Remote Sensing of Environment, vol. 120, pp. 25–36, May 2012, doi: 10.1016/j.rse.2011.11.026.

[38] M. Immitzer, F. Vuolo, and C. Atzberger, “First Experience with Sentinel-2 Data for Crop and Tree Species Classifications in Central Europe,” Remote Sensing, vol. 8, no. 3, p. 166, Feb. 2016, doi: 10.3390/rs8030166.

[39] D. P. Roy et al., “Landsat-8: Science and product vision for terrestrial global change research,” Remote Sensing of Environment, vol. 145, pp. 154–172, Apr. 2014, doi: 10.1016/j.rse.2014.02.001.

[40] M. G. Tuğaç, F. F. Şimşek, and H. Torunlar, “Classification of Agricultural Crops with Random Forest and Support Vector Machine Algorithms Using Sentinel-2 and Landsat-8 Images,” International Journal of Environment and Geoinformatics, vol. 11, no. 3, pp. 106–118, Sept. 2024, doi: 10.30897/ijegeo.1479116.

[41] C. Zhang et al., “An object-based convolutional neural network (OCNN) for urban land use classification,” Remote Sensing of Environment, vol. 216, pp. 57–70, Oct. 2018, doi: 10.1016/j.rse.2018.06.034.

[42] T. Kavzoglu and P. M. Mather, “The use of backpropagating artificial neural networks in land cover classification,” International Journal of Remote Sensing, vol. 24, no. 23, pp. 4907–4938, Jan. 2003, doi: 10.1080/0143116031000114851.

[43] M. Kasahun and A. Legesse, “Machine learning for urban land use/ cover mapping: Comparison of artificial neural network, random forest and support vector machine, a case study of Dilla town,” Heliyon, vol. 10, no. 20, p. e39146, Oct. 2024, doi: 10.1016/j.heliyon.2024.e39146.

[44] S. Talukdar et al., “Land-Use Land-Cover Classification by Machine Learning Classifiers for Satellite Observations—A Review,” Remote Sensing, vol. 12, no. 7, p. 1135, Apr. 2020, doi: 10.3390/rs12071135

## 8 AUTHORS

**Prof. (Mrs) E.O Makinde** is the first female professor in the Department of Surveying and Geoinformatics at the University of Lagos, Nigeria. (Email: eomakinde@unilag.edu.ng; estherdanisi@gmail.com)

**Abdul Hikmat T.** is a Graduate student in the Department of Surveying and Geoinformatics at the University of Lagos, Nigeria. Her areas of interest are Machine learning, GIS and Remote Sensing.

**Oyewole Ayomide P.** is a Graduate student in the Department of Surveying and Geoinformatics at the University of Lagos, Nigeria. His areas of interest are GIS, Remote Sensing, Ocean Mapping, Machine Learning and Artificial Intelligence